

Vesicle electrohydrodynamics

Jonathan T. Schwalbe,¹ Petia M. Vlahovska,² and Michael J. Miksis¹¹*Department of Engineering Sciences and Applied Mathematics, Northwestern University, Evanston, Illinois 60202, USA*²*School of Engineering, Brown University, Providence, Rhode Island 02912, USA*

(Received 8 November 2010; published 20 April 2011)

A small amplitude perturbation analysis is developed to describe the effect of a uniform electric field on the dynamics of a lipid bilayer vesicle in a simple shear flow. All media are treated as leaky dielectrics and fluid motion is described by the Stokes equations. The instantaneous vesicle shape is obtained by balancing electric, hydrodynamic, bending, and tension stresses exerted on the membrane. We find that in the absence of ambient shear flow, it is possible that an applied stepwise uniform dc electric field could cause the vesicle shape to evolve from oblate to prolate over time if the encapsulated fluid is less conducting than the suspending fluid. For a vesicle in ambient shear flow, the electric field damps the tumbling motion, leading to a stable tank-treading state.

DOI: [10.1103/PhysRevE.83.046309](https://doi.org/10.1103/PhysRevE.83.046309)

PACS number(s): 47.20.Ma, 47.57.jd, 87.16.dj

I. INTRODUCTION

Membranes that encapsulate cells and internal cellular organelles are composed primarily of lipid bilayers [1]. Giant unilamellar vesicles (GUVs), which are cell-size membrane envelopes, have gained popularity as models of protocells [2] and systems to study membrane biophysics [3]. Because of their large size (10–100 μm), direct observation is possible of the dynamic features of individual membrane vesicles in real time with optical microscopy. GUVs exhibit rich dynamic behavior in flow or electric fields—see, for example, the reviews in Refs. [4–7]. Understanding the effects of flow on GUVs and cells is fundamental to many naturally occurring biological processes, e.g., blood flow. Applied electric fields are of interest because of their use in biomedical technologies, e.g., gene transfection. In particular, a controlled application of an electric pulse can induce transient pores in the cell or vesicle membrane, which can reseal after the pulse is turned off but may allow the delivery of exogenous molecules. Here we also investigate the combined effect of both flow and an applied dc electric field on the dynamics of a vesicle, which is motivated by the potential use of vesicles as microreactors in micro- and nanofluidic designs, in which complex networks of lipid nanotubes connect vesicle containers [8]. Unlike the conventional microfluidic structures, these “soft” networks can be reconfigured and manipulated by flow or electric fields.

In simple shear flow, a vesicle exhibits several different types of motions. A key physical parameter affecting the dynamics is the viscosity ratio between the fluid outside to the fluid inside the vesicle. With varying viscosity ratio, three of the observed dynamics are [9–13]: (1) *tank treading* (TT), in which the vesicle deforms into a prolate ellipsoid and the membrane rotates as a tank tread, the vesicle major axis is tilted with respect to the flow direction and the inclination angle remains fixed in time; (2) *tumbling* (TB), in which the vesicle undergoes a periodic flipping motion; and (3) *vacillating breathing* (VB) also called *trembling*, where the vesicle is trembling in the flow direction with periodic shape deformations.

A vesicle deforms into an ellipsoid when subjected to a uniform electric field [14–18]. Depending on the conductivity mismatch between the inner and outer fluids, and in the case of the ac field, its frequency, the ellipsoid is prolate or oblate

and its major axis is either collinear with or perpendicular to the applied electric field [17,19]. In this paper, we investigate vesicle response to a dc field and the time evolution of the vesicle shape.

If a simple shear flow and electric field are simultaneously applied, vesicle deformation and orientation become dependent on the relative strength of the electric and shear stresses. For example, an electric field applied along the velocity gradient acts to elongate and align the vesicle perpendicularly to the flow direction, while the shear flow tends to orient the vesicle along the flow direction. This problem, however, has been analyzed only to a limited extent for drops and capsules [20–23]. Thus, another goal of this paper is to theoretically investigate the effect of the competition between electric stress and shear stress on vesicle dynamics. While the behavior of an isolated vesicle in either a uniform electric field [24] or a shear flow [25–28] has been extensively studied, the effect of a combined uniform electric field and fluid flow on vesicle dynamics has, to the best of our knowledge, received no attention. Our study is also motivated by the possible use of electric fields to modulate rheology of vesicle suspensions, and in a more general context to use electrohydrodynamics for cell manipulation.

The theoretical analysis of vesicles in external flows is complicated by the elasto- and electromechanics of the lipid bilayer membrane. Several features of lipid membranes can be identified which underlie the complexity of the problem: (1) Lipid molecules are free to move in the plane of the membrane thus the lipid bilayer behaves as a fluid. (2) Under stress, lipid bilayers store elastic energy in bending, while membranes made of crosslinked polymers are more likely to be stretched and sheared. (3) The lipid bilayer contains a fixed number of molecules and the membrane is nearly area incompressible. In response to in-plane stresses, it develops nonuniform tension, which adapts itself to the forces exerted on the membrane in order to keep the local area constant. (4) The lipid membrane is essentially an insulating shell impermeable to ions. When an electric field is applied, charges accumulate on both sides of the bilayer and the membrane acts as a charging capacitor. In addition, since membranes are embedded in a fluid environment, changes in membrane conformation are coupled to a motion in the surrounding fluids.

Since membranes are molecularly thin, to describe the membrane-fluid coupling it is convenient to use an effective two-dimensional description of the membrane mechanics [29]. The simplest account for the bending stresses comes from the classic Helfrich–Canham energy [30,31]. In this paper we develop an effective zero-thickness model for a fluid-embedded lipid membrane in an electric field and apply it to study vesicle dynamics in a combined shear flow and uniform electric fields.

II. PROBLEM FORMULATION

A. The physical picture: Characteristic time scales, relevant parameters, and their magnitudes

Let us consider a neutrally buoyant vesicle made of a charge-free lipid bilayer membrane with conductivity σ_m and dielectric constant ϵ_m . The bilayer thickness is $h \sim 5$ nm, thus on the length scale of a cell-size vesicle (radius $a \sim 10 \mu\text{m}$) the bilayer membrane can be regarded as a two-dimensional surface with capacitance $C_m = \epsilon_m/h$ and conductivity $G_m = \sigma_m/h$. The vesicle is filled with a fluid of viscosity μ_{in} , conductivity σ_{in} , and dielectric constant ϵ_{in} , and suspended in a different fluid characterized by μ_{ex} , σ_{ex} , and ϵ_{ex} . To characterize the mismatch in the fluid physical properties, we introduce the ratios

$$\Lambda = \frac{\sigma_{in}}{\sigma_{ex}}, \quad S = \frac{\epsilon_{in}}{\epsilon_{ex}}, \quad \eta = \frac{\mu_{in}}{\mu_{ex}}. \quad (1)$$

The departure of the vesicle shape from a sphere is quantified by the excess area, which is the difference between the vesicle area and the area of an equivalent-volume sphere [32],

$$\Delta = A/a^2 - 4\pi, \quad a = \left(\frac{3v}{4\pi}\right)^{1/3}. \quad (2)$$

Here A and v are the true surface area and volume of the vesicle.

The vesicle is subjected to a linear flow with strain-rate magnitude $\dot{\gamma}$ and a uniform dc electric field with magnitude E_0 ,

$$\mathbf{u}^\infty = \dot{\gamma}y\hat{\mathbf{x}}, \quad \mathbf{E}^\infty = E_0\hat{\mathbf{y}}. \quad (3)$$

The vesicle shape can be described by the radial position of the interface $r_s = a(1 + f(\theta, \phi, t))$, where $f(\theta, \phi, t)$ is to be determined as part of the solution. The problem is sketched in Fig. 1.

When an electric field $E(t)$ is applied to an electrolyte solution, ions move. The ion redistribution leads to inhomogeneities in the bulk charge density, which decay on a time scale related to bulk conduction [33,34],

$$t_{c,in} = \frac{\epsilon_{in}}{\sigma_{in}}, \quad t_{c,ex} = \frac{\epsilon_{ex}}{\sigma_{ex}}. \quad (4)$$

Free charges accumulate at boundaries that separate media with different electric properties as illustrated in Fig. 2. The rate of charge buildup at the interface of a macroscopic object, e.g., a sphere, is given by the Maxwell-Wagner polarization time [35],

$$t_{MW} = \frac{\epsilon_{in} + 2\epsilon_{ex}}{\sigma_{in} + 2\sigma_{ex}}. \quad (5)$$

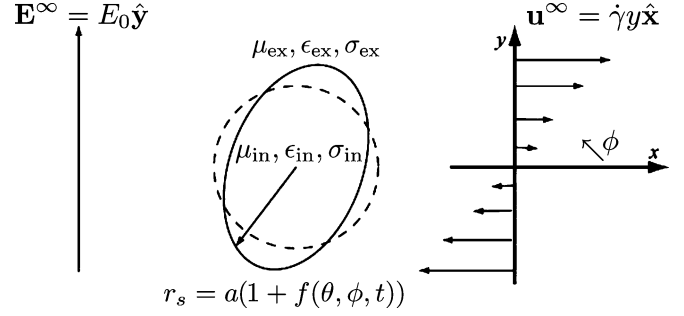


FIG. 1. Sketch of the the problem: a vesicle subjected to a combination of shear flow and a uniform electric field.

The polarization depends on $t_{c,in}/t_{c,ex} = \Lambda/S$. Consider, for example, a droplet suspended in another liquid. The charge relaxation time, t_c , measures how fast conduction supplies charges to restore equilibrium. If $t_{c,in} < t_{c,ex}$, the conduction in the drop is faster than the suspending liquid. As a result, the interface acquires charge dominated by ions brought from the interior fluid and the induced dipole is aligned with the electric field. In this case, charges at the poles are attracted by the electrodes, pulling the drop into a prolate shape. In the opposite case, $t_{c,in} > t_{c,ex}$, the charging response of the exterior fluid is faster than the interior fluid. Hence, the interface charge is dominated by the exterior ions and the polarization is reversed. In this induced-charge configuration, a drop can become an oblate ellipsoid [36]. The lipid membrane, however, represents a more complex boundary compared to fluid-fluid interfaces. It is impermeable to ions and, therefore, charges accumulate on both the inner and outer physical surfaces. Hence, the vesicle acts as a capacitor that charges on a time scale given by [37–39]

$$t_m = aC_m \left(\frac{1}{\sigma_{in}} + \frac{1}{2\sigma_{ex}} \right). \quad (6)$$

For simplicity, the vesicle is modeled as a spherical insulating shell. The membrane capacitance gives rise to a potential difference across the membrane and a capacitive current through the membrane.

If the electric field is not normal to the interface, its tangential component acts on the induced free charges at the interface and gives rise to a shearing force. This is illustrated in Fig. 2 on the example of a spherical droplet. The electrical force drags the interface in motion. The resulting electrohydrodynamic (EHD) flow is characterized by a time

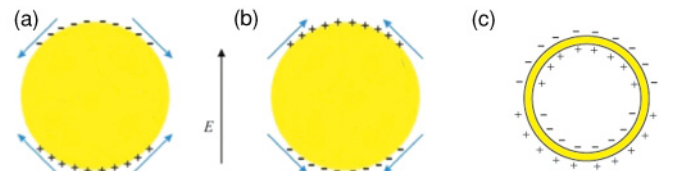


FIG. 2. Surface charge distribution and direction of the surface electric force for a sphere with (a) $t_{c,in} > t_{c,ex}$ and (b) $t_{c,in} < t_{c,ex}$. (c) Sketch of the induced charge distribution around a spherical insulating shell.

scale, which corresponds to the inverse of the shear rate imposed by the tangential electric stress,

$$t_{el} = \frac{\mu_{ex}(1 + \eta)}{\epsilon_{ex}E_0^2}. \quad (7)$$

The straining component of the external shear flow also distorts vesicle shape by elongating it along the extensional axis of the flow, which is oriented at a 45° angle relative to the flow direction. The corresponding time scale is $t_e = (1 + \eta)\dot{\gamma}^{-1}$.

Vesicle deformation by electric and flow stresses is limited by the membrane's resistance to bending and stretching. A distortion in the vesicle shape relaxes on a time scale

$$t_\kappa = \frac{\mu_{ex}(1 + \eta)a^3}{\kappa}, \quad (8)$$

where κ is the bending modulus. The curvature relaxation depends on the average viscosities of the bulk fluids, because viscous dissipation on length scales greater than a micrometer takes place in the bulk [40].

The ratio of distorting electric and restoring bending time scales defines a capillarylike number,

$$Ca = \frac{t_\kappa}{t_{el}} \equiv \frac{\epsilon_{ex}E_0^2a^3}{\kappa}. \quad (9)$$

It is convenient to introduce a dimensionless number, which is independent of the membrane properties:

$$Mn = \frac{\epsilon_{ex}E_0^2}{\mu_{ex}\dot{\gamma}}. \quad (10)$$

The Mason parameter, Mn , compares the strength of electric and viscous stresses.

Let us estimate the magnitude of the above time scales involved in the process of vesicle electrodeformation. Typical experimental conditions involve solutions with conductivities in the range $\sigma \sim 10^{-4}$ S/m and electric fields of the order of $E \sim 1$ kV/cm [14–19,41–46]. The typical size of a giant vesicle is $a \sim 10$ μ m. The inner and outer fluids are essentially water: viscosity $\mu \sim 10^{-3}$ Pa s, and density $\rho \sim 1000$ kg/m³. The membrane capacitance is $C_m \sim 10^{-2}$ F/m² [47] and bending rigidity $\kappa \sim 10^{-19}$ J. Therefore, for vesicles, we estimate the basic charging time and the Maxwell-Wagner polarization time to be of the same order $t_c \sim t_{MW} \sim 10^{-6}$ s, the membrane charging time is $t_m \sim 10^{-3}$ s, the electrohydrodynamic time is $t_{el} \sim 10^{-2}$ s, and the bending relaxation time is $t_\kappa \sim 10$ s. Typical shear rates range from $\dot{\gamma} \sim 0.1$ to 100 s⁻¹ [48–51].

We see that the vesicle electrohydrodynamics involves processes that occur on very different time scales. Bulk phases become electroneutral on a time scale given by charge relaxation time (4), and charging of the interface occurs on a similarly fast time scale (5). Hence, we can assume a quasistatic electric field. However, the electric field can vary with time as the membrane capacitor charges. These variations can take place on a time scale comparable to vesicle response to imposed shear flow ($t_m \sim \dot{\gamma}^{-1}$), or electric field ($t_m \sim t_{el}$), rendering the problem intrinsically nonlinear and time dependent.

B. Governing equations

We adopt the leaky dielectric model, which combines the Stokes equations to describe fluid motion with conservation of current described by Ohm's law [34]. Under the assumption of charge-free fluids, the electric and hydrodynamic fields are decoupled in the bulk.

The pressure, p , and the fluid velocity, \mathbf{u} , fields obey

$$\begin{aligned} \mu_{in}\nabla^2\mathbf{u}_{in} &= \nabla p_{in}, & \nabla \cdot \mathbf{u}_{in} &= 0, \\ \mu_{ex}\nabla^2\mathbf{u}_{ex} &= \nabla p_{ex}, & \nabla \cdot \mathbf{u}_{ex} &= 0. \end{aligned} \quad (11)$$

In the absence of bilayer slip and membrane permeability, the velocity is continuous across the interface. The shape evolution is determined from the kinematic condition that the interface moves with the normal component of the fluid velocity $\mathbf{u}_{in}(r_s) = \mathbf{u}_{ex}(r_s) \equiv \mathbf{u}_s$,

$$\frac{\partial r_s}{\partial t} = \mathbf{u}_s \cdot \mathbf{n}. \quad (12)$$

The quasistatic electric field, \mathbf{E} , in the absence of bulk charges is irrotational and the electric potential, Φ , satisfies

$$\mathbf{E} = -\nabla\Phi, \quad \nabla^2\Phi = 0. \quad (13)$$

The potential undergoes a jump across a capacitive interface,

$$\Phi_{in} - \Phi_{ex} = V_m. \quad (14)$$

The transmembrane potential, V_m , is determined as part of the problem; in general, it is a complex function of the geometry, and fluid and membrane physical properties. Far away from the vesicle, the velocity \mathbf{u} and electric fields \mathbf{E} tend to the unperturbed flow, $\mathbf{u} \rightarrow \mathbf{u}^\infty$ and electric field, $\mathbf{E} \rightarrow \mathbf{E}^\infty$, respectively.

The electric and flow fields are coupled through the boundary condition for stress balance and current conservation at the interface. The hydrodynamic and electric tractions are discontinuous and are balanced by membrane forces,

$$\mathbf{n} \cdot [(\mathbf{T}_{ex} - \mathbf{T}_{in}) + (\mathbf{T}_{ex}^{el} - \mathbf{T}_{in}^{el})] = \boldsymbol{\tau}^m \quad \text{at } r = r_s, \quad (15)$$

where \mathbf{n} is the outward pointing normal vector. The membrane stresses $\boldsymbol{\tau}^m$ are discussed in Sec. II C. Here $T_{ij} = -p\delta_{ij} + \mu(\partial_j u_i + \partial_i u_j)$ is the bulk hydrodynamic stress and δ_{ij} is the Kronecker delta function. The electric stress is given by the Maxwell stress tensor $T_{ij}^{el} = \epsilon(E_i E_j - E_i E_i \delta_{ij}/2)$.

The current density is continuous across the membrane [52],

$$\mathbf{n} \cdot (\sigma_{ex}\mathbf{E}_{ex}) = \mathbf{n} \cdot (\sigma_{in}\mathbf{E}_{in}) = C_m \frac{dV_m}{dt}. \quad (16)$$

The effective induced charge on the membrane is formally defined as a jump in the displacement fields across the interface,

$$Q = \mathbf{n} \cdot (\epsilon_{ex}\mathbf{E}_{ex} - \epsilon_{in}\mathbf{E}_{in}). \quad (17)$$

In our model of the membrane as a zero-thickness capacitive interface, Q is not the charge of the capacitor; for a fully charged capacitor, $Q = 0$. Q represents the difference between the charge densities on the inner and outer physical surfaces of the membrane. This imbalance occurs because if bulk conductivities differ, charges at the physical surfaces of the membrane are supplied at different rates.

C. Membrane forces

Fluid membranes made of lipid bilayers are governed by resistance to curvature changes. The membrane free energy is

$$\mathcal{F} = \int \left[\frac{\kappa}{2} (2H)^2 + \Sigma \right] dA, \quad (18)$$

where κ is the bending modulus. The membrane tension, Σ , is a Lagrange multiplier that enforces the area incompressibility. The quantity H is the mean curvature of the surface, given by

$$H = \frac{1}{2} \nabla \cdot \mathbf{n}. \quad (19)$$

The corresponding membrane forces are found by taking a variational derivative of (18) [40]

$$\boldsymbol{\tau}^m = \left[-2\kappa(2H^3 - 2K_g H + \nabla_s^2 H) + 2\Sigma H \right] \mathbf{n} - \nabla_s \Sigma, \quad (20)$$

where K_g is the Gaussian curvature of the surface given by

$$K_g = \frac{1}{2} \nabla \cdot [\mathbf{n} \nabla \cdot \mathbf{n} + \mathbf{n} \times (\nabla \times \mathbf{n})]. \quad (21)$$

$\nabla_s = \mathbf{I}_s \cdot \nabla$ is the surface gradient operator, $\mathbf{I}_s = \mathbf{I} - \mathbf{n}\mathbf{n}$ is the surface projection, and $I_{ij} \equiv \delta_{ij}$.

III. SOLUTION FOR A NEARLY SPHERICAL VESICLE

In order to make analytical progress, we consider a vesicle with a small excess area, $\Delta \ll 1$. In this limit the deviation from sphericity, f , scales as $\Delta^{1/2}$. We proceed to determine the leading-order solution. Assuming that the applied electric field scales as $\Delta^{1/4}$ allows us to find the electric field by solving for the potential about a sphere with the boundary condition (16) independent of the flow and vesicle asphericity. The corresponding electric stresses are then inserted in the stress conditions (15) to find the velocity field and the vesicle deformation.

A. Solution outline

Due to the linearity of the Stokes equations, the velocity field can be decomposed into two components: a flow about a vesicle subject to a shear flow (in absence of electric field) and a flow about a vesicle in electric field (in absence of applied shear). The first problem has been solved in Refs. [25] and [26]. Here we derive the solution for the second problem, namely, the electrodeformation of a spherical particle with a capacitive interface. Then we combine the two solutions and explore the vesicle dynamics resulting from the interplay of shear and electric stresses. The solution of the hydrodynamic part is summarized in Appendix E.

As noted earlier, in a spherical coordinate system centered at the vesicle, the position of the interface is

$$r_s(\theta, \phi, t) = a[1 + f(\theta, \phi, t)], \quad (22)$$

where f measures the deviation from sphericity. All variables are expanded in spherical harmonics Y_{jn} (D1). For example,

$$f(\theta, \phi, t) = \sum_{j \geq 2} \sum_{n=-j}^j f_{jn}(t) Y_{jn}. \quad (23)$$

The $j = 1$ modes have been omitted because they describe translation of the center of mass. The order of magnitude of the asphericity ($f \sim \Delta^{1/2}$) becomes evident from the expression for the vesicle's excess area,

$$\Delta = \frac{1}{2} \sum_{j,n} (j+2)(j-1) f_{jn} f_{jn}^* + O(f^3). \quad (24)$$

where the $\sum_{j,n}$ is shorthand notation for the double sum in (23) and the $*$ denotes the complex conjugate, $f_{jn}^* = (-1)^n f_{j,-n}$.

The quasistatic electric field is irrotational, i.e., $\mathbf{E} = -\nabla \Phi$, and the electric potential Φ is a solution of the Laplace equation. Hence, the solutions for the electric field are growing and decaying spherical harmonics, which derive from $\nabla(r^j Y_{jn})$ and $\nabla(r^{-j-1} Y_{jn})$,

$$\begin{aligned} \mathbf{E}_{\text{ex}} &= \mathbf{E}^\infty - \sum_{j,n} P_{jn}^{\text{ex}} \nabla(r^{-j-1} Y_{jn}), \\ \mathbf{E}_{\text{in}} &= - \sum_{j,n} P_{jn}^{\text{in}} \nabla(r^j Y_{jn}). \end{aligned} \quad (25)$$

A uniform electric field applied in the y - z plane (perpendicular to the flow direction) is defined by

$$\mathbf{E}^\infty = E_0(\alpha \hat{\mathbf{y}} + \beta \hat{\mathbf{z}}) = -E_0 \sum_{n=-1}^1 e_{1n}^\infty \nabla(r Y_{1n}), \quad (26)$$

where

$$e_{10}^\infty = \beta \sqrt{\frac{4\pi}{3}}, \quad e_{1\pm 1}^\infty = \alpha i \sqrt{\frac{2\pi}{3}}. \quad (27)$$

B. Electric field and the transmembrane potential

The solution for the electric potential around a sphere placed in a uniform electric field is

$$\begin{aligned} \Phi_{\text{ex}} &= -E_0 \left[r + P_{\text{ex}} \frac{a^3}{r^2} \right] \sum_{n=-1}^1 e_{1n}^\infty Y_{1n}, \\ \Phi_{\text{in}} &= -E_0 P_{\text{in}} r \sum_{n=-1}^1 e_{1n}^\infty Y_{1n}. \end{aligned} \quad (28)$$

Applying the boundary conditions (16) we find

$$P_{\text{ex}} = \frac{(-\Lambda + 1) + \Lambda \bar{V}(t)}{\Lambda + 2}, \quad P_{\text{in}} = \frac{3 - 2\bar{V}(t)}{\Lambda + 2}, \quad (29)$$

where $\bar{V}(t)$ is the amplitude of the transmembrane potential, $V_m = \Phi_{\text{in}}(r = a) - \Phi_{\text{ex}}(r = a) = \bar{V}(t) E_0 a \sum e_{1n}^\infty Y_{1n}$,

$$\bar{V}(t) = \frac{3}{2} \left[1 - \exp\left(-\frac{t}{t_m}\right) \right], \quad (30)$$

where t_m is the membrane charging time defined by Eq. (6). Note that the transmembrane potential is position dependent. Its absolute value is maximal at the poles, i.e., closest to the electrodes. At the equator the transmembrane potential is zero. At steady state, the vesicle interior is ‘‘shielded,’’ i.e., the interior electric field is zero, and the maximal potential

drop across the membrane is $\bar{V} = 1.5$. The effective charge density is calculated from (17)

$$\begin{aligned} Q(t) &= \epsilon_{\text{ex}} E_0 (1 - 2P_{\text{ex}} - SP_{\text{in}}) \sum_{n=-1}^1 e_{1n}^{\infty} Y_{1n} \\ &= \epsilon_{\text{ex}} E_0 \frac{\Lambda - S}{\Lambda + 2} [3 - 2\bar{V}(t)] \sum_{n=-1}^1 e_{1n}^{\infty} Y_{1n} \\ &= \epsilon_{\text{ex}} E_0 \bar{Q}(t) \sum_{n=-1}^1 e_{1n}^{\infty} Y_{1n}. \end{aligned} \quad (31)$$

We see that the effective charge on the membrane decreases as the transmembrane potential increases. At long times, when the capacitor becomes fully charged, the imbalance between the inner and outer surface charge density vanishes and $Q = 0$.

C. Electric stresses

The tractions that the electric field exerts on a sphere, $r = a$, are

$$\begin{aligned} \mathbf{t}^{\text{el}} &= \epsilon_{\text{ex}} [(\hat{\mathbf{r}} \cdot \mathbf{E}_{\text{ex}}) \mathbf{E}_{\text{ex}} - \frac{1}{2} \mathbf{E}_{\text{ex}} \cdot \mathbf{E}_{\text{ex}} \hat{\mathbf{r}}] \\ &\quad - \epsilon_{\text{in}} [(\hat{\mathbf{r}} \cdot \mathbf{E}_{\text{in}}) \mathbf{E}_{\text{in}} - \frac{1}{2} \mathbf{E}_{\text{in}} \cdot \mathbf{E}_{\text{in}} \hat{\mathbf{r}}]. \end{aligned} \quad (32)$$

A uniform electric field with $j = 1$ symmetry generates electric tractions with $j = 0$ and $j = 2$ (see Appendix D). The isotropic part $j = 0$ is balanced by the hydrostatic pressure and does not lead to deformation. Only the position-dependent stress leads to vesicle deformation,

$$\mathbf{t}^{\text{el}} = \epsilon_{\text{ex}} E_0^2 (p^{\text{el}} \hat{\mathbf{r}} + \boldsymbol{\tau}^s). \quad (33)$$

The dimensionless electric pressure is

$$p^{\text{el}} = -\bar{p} [3\alpha^2 \cos 2\phi \sin^2 \theta + \frac{1}{2}(\alpha^2 - 2\beta^2)(1 + 3 \cos 2\theta)]. \quad (34)$$

The dimensionless tangential electric traction is

$$\begin{aligned} \boldsymbol{\tau}^s &= \bar{\tau}^s \{-\alpha^2 \sin \theta \sin 2\phi \mathbf{e}_\phi + \frac{1}{2}[\alpha^2(\cos 2\phi - 1) \\ &\quad + 2\beta^2] \sin 2\theta \mathbf{e}_\theta\}. \end{aligned} \quad (35)$$

We have explicitly shown the angular dependence of the pressure and tangential stress; the amplitudes \bar{p} and $\bar{\tau}^s$ depend solely on the physical parameters of the system such as Λ , S . The amplitude of the radial (pressure) component is given by

$$\bar{p} = \frac{1}{12} [2 - 2P_{\text{ex}} + 5P_{\text{ex}}^2 - 2SP_{\text{in}}^2], \quad (36)$$

and the tangential (shearing) component is

$$\bar{\tau}^s = \frac{1}{2} [-1 + P_{\text{ex}} + 2P_{\text{ex}}^2 + SP_{\text{in}}^2]. \quad (37)$$

With the electrostatic problem solved, we next proceed to compute vesicle deformation in response to an electric field.

IV. VESICLE DYNAMICS IN ABSENCE OF APPLIED SHEAR FLOW

In this section, all quantities are nondimensionalized using the capacitor charging time t_m , and the characteristic

magnitude of the bulk electric stress $\epsilon_{\text{ex}} E_0^2$. Casting equations in dimensionless form helps capture the physical picture in a broader class of situations rather than just one set of dimensional parameters.

At leading order (linear response), the vesicle shape has the same symmetry as the deformation-inducing electric stresses, i.e., $j = 2$. The evolution equations for the shape parameters f_{2n} for a vesicle in an electric field oriented in an arbitrary direction are [7,24,53]

$$\delta_m \frac{df_{2n}}{dt} = C_{2n}^{\text{el}} - \text{Ca}^{-1} R_2 f_{2n}. \quad (38)$$

where $\delta_m = t_{\text{el}}/t_m$ compares the time it takes to deform the vesicle relative to the time it takes to charge the membrane capacitor.

The inhomogeneous term represents shape distortion by the applied electric field. For simplicity, let us consider a field oriented along the z direction (the corresponding expressions for a field in the y direction are listed in Appendix A):

$$C_{20}^{\text{el}} = \frac{16\sqrt{5\pi}(3\bar{p} - \bar{\tau}^s)}{5(32 + 23\eta)}, \quad (39)$$

The full expression for C_{20}^{el} is given by (A1).

The term proportional to Ca^{-1} in (38) describes the relaxation of the shape by bending stresses and the isotropic part of the membrane tension,

$$R_2 = \frac{24(6 + \Sigma_h)}{32 + 23\eta}. \quad (40)$$

The membrane tension Σ_h depends on the instantaneous vesicle shape and is determined self-consistently with deformation to keep the total area constant [26]—see Appendix E for details. The leading-order shape evolution equation becomes quadratic in the shape parameter f in contrast to the corresponding results for drops [36]. This feature of nonequilibrium vesicle dynamics has been noted by several authors in relation to vesicle dynamics in shear flow [25–27].

Inserting (40) and the expression for the tension Σ_h (E20) in (38) leads to

$$\begin{aligned} \delta_m \frac{df_{20}}{dt} &= C_{20}^{\text{el}}(t) (1 - 2\Delta^{-1} f_{20}^2), \\ \delta_m \frac{df_{2n}}{dt} &= -2C_{20}^{\text{el}}(t) \Delta^{-1} f_{20} f_{2n}. \end{aligned} \quad (41)$$

Note that rescaling the time by the membrane capacitor charging time collapses all curves for vesicle shape as function of time on a universal plot for a given δ_m .

The f_{2n} modes are slaved to the f_{20} shape mode, which is forced to change by the electric field. An analytic solution for f_{20} can be found from the first equation in (41),

$$f_{20}(t) = \sqrt{\frac{\Delta}{2}} \tanh \left[\sqrt{\frac{2}{\Delta}} \frac{1}{\delta_m} J(t) \right], \quad (42)$$

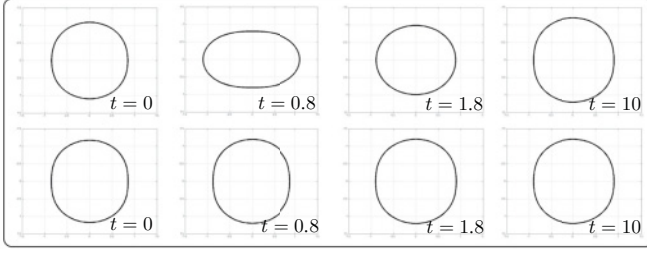


FIG. 3. Contours of the vesicle shape in the x - z plane. The top row is for a conductivity ratio of $\Lambda = 10$, and the bottom is for $\Lambda = 0.1$. Both solutions are with $\delta_m = 1$ and $\eta = 1$. The initial conditions for the $f_{2\pm 2} = f'_{22} \pm i f''_{22}$ are $f'_{22}(0) = f''_{22}(0) = \sqrt{0.1\Delta}$. The f_{20} mode is determined from Eq. (24) with $\Delta = 0.2$.

where $f_{20}(0) = 0$ was chosen as the initial condition, and

$$J(t) = \int_0^t C_{20}^{\text{el}}(s) ds = B_1 \{ B_2 + B_3 t + \exp(-2t)[B_4 - B_5 \exp(t)] \}. \quad (43)$$

The constant B_k terms are listed in Appendix B [see Eq. (B1)]. Equations (41) and (42) show that the maximum possible deformation of f_{20} is

$$f_{20}^{\text{max}} = \pm \sqrt{\frac{\Delta}{2}}, \quad (44)$$

which simply states that all excess area is transferred into the f_{20} mode at long times, $t \rightarrow \infty$. A positive f_{20} is characteristic of the prolate configuration, while when $f_{20} < 0$, the vesicle is in the oblate configuration.

Figure 3 illustrates the time-dependent shape dynamics obtained from (41) upon a stepwise application of an uniform dc field. We observe that if $\Lambda < 1$ (and $S = 1$), the vesicle deforms initially into an oblate ellipsoid and then into a prolate ellipsoid. Equation (42) and (43) [or just (41)] show that the type of deformation can only change from oblate to prolate if $C_{20}^{\text{el}}(t)$ changes sign. Setting $C_{20}^{\text{el}}(t) = 0$ and solving for the time t we find that

$$t_{\text{ob}} = t_m \log \left[\frac{4\sqrt{S} - \Lambda}{2 + \Lambda} \right]. \quad (45)$$

Since time cannot be negative, the argument of the log function has to be greater than 1. Hence, this condition shows that a change in shape is possible if

$$\Lambda < 2\sqrt{S} - 1. \quad (46)$$

If $S = 1$, which is the typical case for vesicle experiments, we find that $\Lambda < 1$ in order to have oblate-prolate transition. This conclusion also is in accordance with similar analysis for the oblate-prolate transition of vesicles in a uniform ac electric field with decreasing frequency [24,54,55].

Equation (45) also shows that increasing the membrane capacitance δ_m increases the time the vesicle spends in the oblate state. Fixing S and δ_m and decreasing Λ toward zero, also prolongs t_{ob} .

To gain better physical insight into the mechanisms of the oblate-prolate transition, Fig. 4 parallels the time evolution

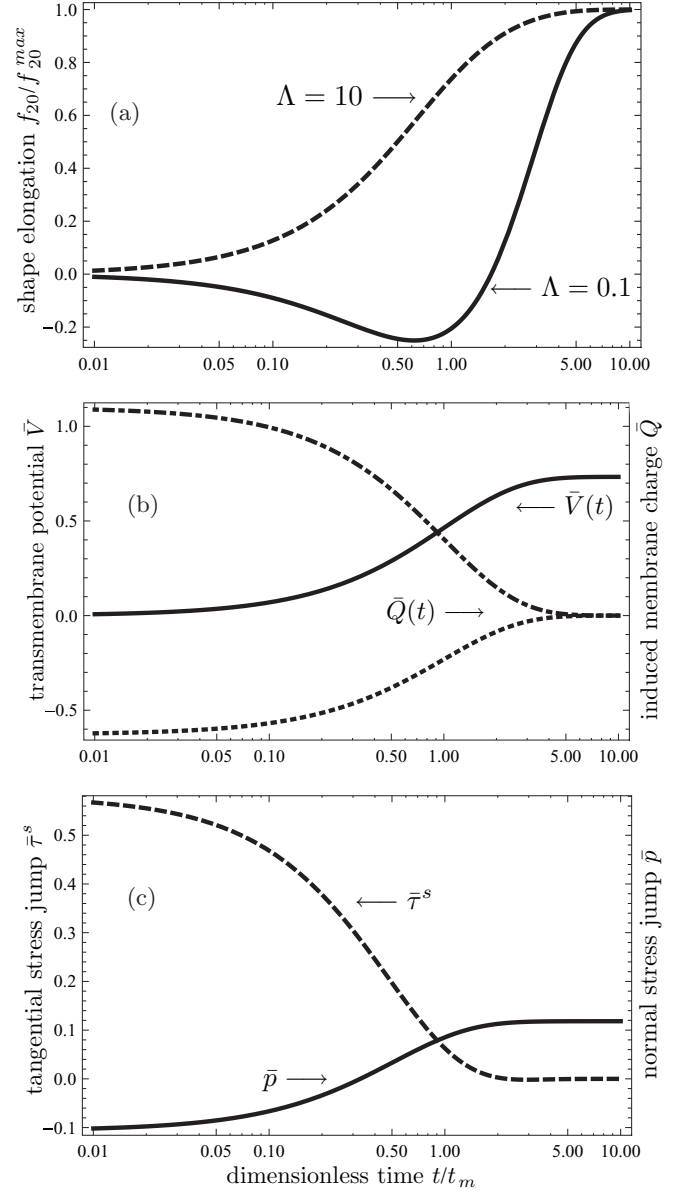


FIG. 4. (a) Evolution of the ellipsoidal deformation $f_{20}/f_{20}^{\text{max}}$ of a quasispherical vesicle upon application of a uniform dc electric field. The solid and dashed curves are with $\Lambda = 0.1$, and 10, respectively. (b) Evolution of the transmembrane potential, computed from (30), and the effective charge computed from (31) [dotted line ($\Lambda = 0.1$) and dotted-dashed line ($\Lambda = 10$)]. (c) Electric pressure (solid line) and shear stress (dashed line). Parameter values are $\Lambda = 0.1$, $S = 1$. Time is nondimensionalized by the capacitor charging time and for all calculations, $\delta_m = 1$.

of the f_{20} shape mode, the induced charge, and the transmembrane potential. In the case $\Lambda < 1$, initially the induced effective surface charge is nonzero and the deformation is of oblate type. As time progresses and the membrane capacitor charges, the imbalance in the charge densities on the two membrane surfaces diminishes. Once the capacitor becomes fully charged, the effective surface charge vanishes, and the transmembrane potential reaches its steady-state maximum value. The interior electric fields also vanishes and the vesicle assumes a prolate shape.

V. VESICLE DYNAMICS IN A COMBINED ELECTRIC FIELD AND SHEAR FLOW

In this section, the time scale is $\dot{\gamma}^{-1}$, the velocity scale is $a\dot{\gamma}$, and bulk flow stresses are scaled with $\mu_{\text{ex}}\dot{\gamma}$. The scaling of the electric charge and electric stresses remains unchanged.

The evolution equation for the shape deformation modes f_{2n} is obtained from (E17) in conjunction with (E18)–(E20). In the absence of an electric field, these equations are derived in Ref. [26]. The electric field modifies the forcing term and the tension [23,53],

$$\begin{aligned} \frac{df_{2n}}{dt} = & \frac{in}{2} f_{2n} + C_{2n}^{\text{shear}} + \text{Mn} C_{2n}^{\text{el}} \\ & - \text{Ca}_{\dot{\gamma}}^{-1} \frac{24[6 + \Sigma_h(f_{2n})]}{23\eta + 32} f_{2n}. \end{aligned} \quad (47)$$

where $\text{Ca}_{\dot{\gamma}}$ compares the magnitude of the bending and shear flow stresses, $\text{Ca}_{\dot{\gamma}} = \mu_{\text{ex}}\dot{\gamma}a^3/\kappa$. The Mason number Mn defined by (10) compares the relative strength of the applied shear and electric fields; $\text{Mn} = 0$ corresponds to vesicle in shear flow and no electric field [26].

The forcing by the electric field is given by (A1) for a field applied in the vorticity (z) direction and (A2) for a field applied in the velocity gradient (y) direction. The contribution from the simple shear flow has been derived in Ref. [26]:

$$C_{2n}^{\text{shear}} = -in \frac{2\sqrt{30\pi}}{23\eta + 32}. \quad (48)$$

The electric field adds to the shear flow forcing, thereby increasing the membrane (TT) velocity. Moreover, the electric field decreases the membrane tension (E20), because it excites deformation along the vorticity direction (specified by f_{20} mode),

$$\begin{aligned} \Sigma_h = & -6 + \text{Ca}_{\dot{\gamma}} \frac{32 + 23\eta}{12} [\text{Mn} C_{20}^{\text{el}} f_{20} \\ & + (C_{22}^{\text{shear}} + \text{Mn} C_{22}^{\text{el}}) f_{2-2} \\ & + (C_{2-2}^{\text{shear}} + \text{Mn} C_{2-2}^{\text{el}}) f_{22}]. \end{aligned} \quad (49)$$

Physically, in the presence of electric field the vesicle's contour in the shear plane is rounder due to the additional electric pressure (34). It perturbs the applied shear streamlines less and hence the vesicle's propensity to tumble decreases. We will see in Sec. VB that indeed the electric field suppresses the TT-TB transition.

Inserting (49) in (47) leads to

$$\frac{df_{2n}}{dt} = \frac{in}{2} f_{2n} + C_{2n} - 2\Delta^{-1} f_{2n} \sum_{n=-2}^2 f_{2n}^* C_{2n}, \quad (50)$$

where

$$C_{2n} = C_{2n}^{\text{shear}} + \text{Mn} C_{2n}^{\text{el}}. \quad (51)$$

Instead of shape modes, the vesicle dynamics can be also conveniently described in terms of the orientation angle, ψ , and R , which measures the ellipticity of the vesicle contour in the x - y plane [25],

$$f_{2\pm 2} = R \exp(\mp 2i\psi). \quad (52)$$

The f_{20} mode can be determined from the area constraint (24),

$$f_{20} = \left[\frac{\Delta}{2} - 2f_{22}f_{2-2} \right]^{1/2} = \left[\frac{\Delta}{2} - 2R^2 \right]^{1/2}. \quad (53)$$

Thus we obtain for the evolution equations for the shape and orientation of a fluid membrane vesicle,

$$\frac{d\psi}{dt} = -\frac{1}{2} - \frac{C_{22}''}{2R(t)} \cos[2\psi(t)] - \frac{C_{22}'}{2R(t)} \sin[2\psi(t)], \quad (54)$$

$$\begin{aligned} \frac{dR}{dt} = & \left(1 - 4 \frac{R(t)^2}{\Delta} \right) \{ C_{22}' \cos[2\psi(t)] - C_{22}'' \sin[2\psi(t)] \} \\ & - 2C_{20}R(t)\Delta^{-1} \left[\frac{\Delta}{2} - 2R^2 \right]^{1/2}, \end{aligned} \quad (55)$$

where $C_{22} = C_{22}' + iC_{22}''$. Note that in the absence of an electric field ($C_{20} = C_{22}' = 0$) and R constant, (54) reduces to the Keller-Skalak equation describing the dynamics of a TT ellipsoid [56]. In the next sections we analyze the vesicle motions described by the above equations in the absence and presence of electric field.

A. No electric field

For the sake of completeness, here we summarize the results for vesicle dynamics in simple shear flow. In the absence of electric field, $C_{20} = C_{22}' = 0$, and $C_{22}'' = -4\sqrt{30\pi}/(23\eta + 32)$ [25]. In this case, the set of coupled nonlinear equations has a stable fixed point corresponding to the TT state [$R^* = \sqrt{\Delta}/2$, $\cos(2\psi^*) = -\sqrt{\Delta}/2C_{22}''$] or a closed orbit centered at ($\psi^* = 0$, $R^* = -C_{22}''$) describing the breathing mode. Tumbling does not correspond to an equilibrium point. The TT fixed point loses stability at a critical viscosity ratio,

$$\eta_c = -\frac{32}{23} + \frac{120}{23} \sqrt{\frac{2\pi}{15\Delta}}. \quad (56)$$

Physically, in the absence of electric field, at $\eta < \eta_c$ the torque of the applied shear flow is transmitted via the TT membrane into circulation of the interior fluid and the vesicle assumes a stationary TT state. However, at high interior fluid viscosity, $\eta > \eta_c$, the fluid flows less readily and the interior fluid circulation cannot compensate the shear torque; the vesicle TT state becomes unstable and the vesicle responds by executing rigid body rotation (tumbling).

If there is no deformation along the vorticity direction, i.e., $f_{20} = 0$ at all times, Eq. (53) implies that R remains constant and equal to its maximum value $\sqrt{\Delta}/2$. This situation resembles the Keller-Skalak model [56]: The vesicle shape is a fixed ellipsoid and the vesicle dynamics is described only by the variations of the angle ψ (note, however, that unlike the Keller-Skalak solution, our velocity field is strictly area incompressible). The nonlinear dynamics (either VB or TB) for $\eta > \eta_c$ will depend on the amplitude of the oscillation and the value of η . For example, in Ref. [26], results are presented which show a VB motion with large amplitude variation in f_{20} for η slightly greater than critical, while the dynamics become TB, with small amplitude variation of f_{20} , for values of η much larger than critical. In the breathing mode, the vesicle undergoes periodic shape deformations along the vorticity direction and appears to tremble in the flow direction.

B. Combined electric field and shear flow

The presence of the electric field modifies the vesicle dynamics in shear flow. Let us consider the case of an electric field applied in the velocity gradient (y) direction.

The steady TT state of the vesicle depends on strength of the electric field, as seen in Fig. 5. For example, the inclination angle of the vesicle major axis with respect to the flow direction increases. This effect is illustrated in Fig. 5(b). As Mn increases, ψ increases toward $\pi/2$, the orientation of the applied electric field with respect to the flow direction (x axis).

In the previous section we saw that in the absence of the electric field, increasing the viscosity contrast η brings the vesicle into the tumbling regime which is characterized by a periodic variation of the f_{2n} modes. In the presence of an electric field, this periodic motion is damped because the electric field generates a torque, which opposes the shear one. The electric field acting to align the vesicle major axis with the field stabilizes the TT state.

Figure 6(a) illustrates the vesicle tumbling with decaying amplitude toward the TT configuration. Increasing the viscosity of the vesicle, which enhances the viscous forces acting on

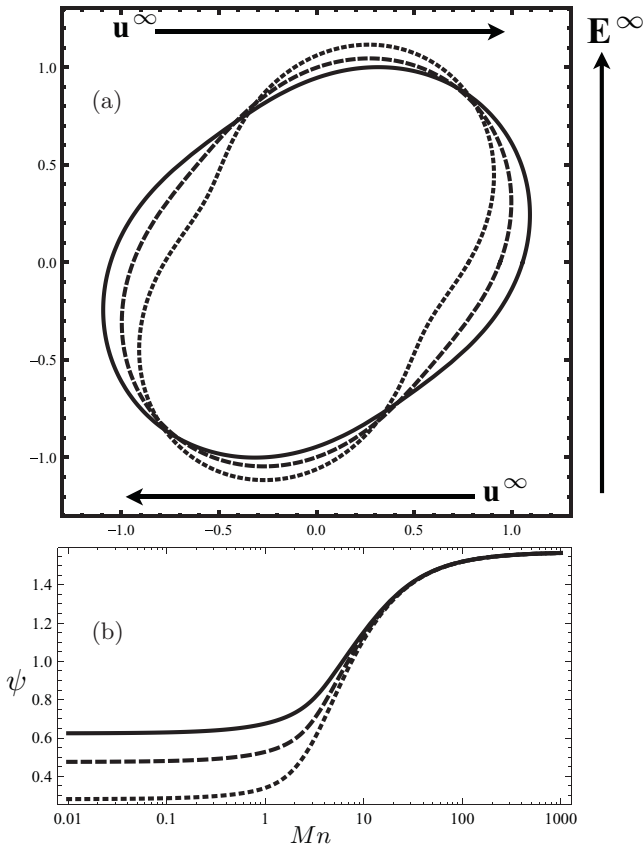


FIG. 5. (a) Contours of the vesicle viewed in the x - y plane for $\eta = 1$. The vesicle is stressed by the combined shear flow, and electric field in the y direction ($\alpha = 1, \beta = 0$). The solid, dashed, and dotted contours are with $Mn = 0, Mn = 5$, and $Mn = 12$, respectively. The remaining parameters are $\Lambda = 10, S = 1, \delta_m = 10$, and $\Delta = 0.2$. The initial conditions are the same as those in Fig. 3. (b) Inclination angle of vesicle at various Mn . The solid, dashed, and dotted curves are with $\eta = 1, 3$, and 5 , respectively.

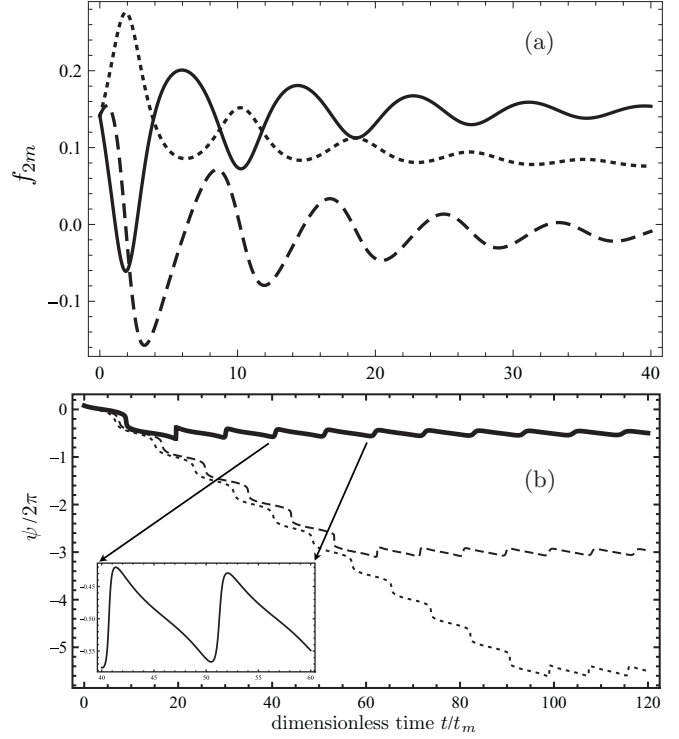


FIG. 6. (a) Time dependence of the f_{2n} modes in the damped tumbling state. The solid, dashed, and dotted curves are f_{22}'', f_{22}' , and f_{20} , respectively with $\eta = 10$. The remaining parameters are $\Lambda = 10, \delta_m = 10, S = 1, Mn = 0.25$, and $\Delta = 0.2$. (b) Time dependence of ψ . The solid, dashed, and dotted curves are, respectively, with $\eta = 8, 9$, and 10 . The remaining parameters are the same as those in (a).

the vesicle, only lengthens the time required for the electric stresses to fully dampen the tumbling motion. This effect is seen in Fig. 6(b), where ψ is shown at various η . During the damped tumbling motion, the vesicle rotates clockwise, and ψ will increase negatively until the electric stresses have overcome tumbling motion, and the major axis can no longer make a complete rotation. The total number of rotations is therefore given by $\psi/2\pi$.

A linear stability analysis can be performed for $Mn > 0$ in the long-time limit where the time-dependent coefficients are constant. Here the analysis is performed using the 3×3 system of Eq. (50). This choice was made in order to remain consistent with the discussion at the end of Sec. IV, where the system given by (41) (dynamics described by shape modes) was used in the stability discussion. Figure 7 illustrates the stability of the system by examining the dependence of the eigenvalues on the viscosity ratio. For viscosity ratios η less than some critical value η_e , there are three negative real eigenvalues, implying stability. For $\eta > \eta_e$, two of the real eigenvalues become complex conjugates; however, the real part is negative, which implies stability. From these numerical results, we conclude that the same steady-state solution is stable for all values of η , but how this solution is approached depends on η . For small η we see a stable node, while if $\eta > \eta_e$, there is a damped oscillation into the TT solution. It is interesting to note that the computed value of $\eta_e \approx 4$ is less than the critical η for the $Mn = 0$ case given in Eq. (56), $\eta_c = 6.15$, implying the η_e

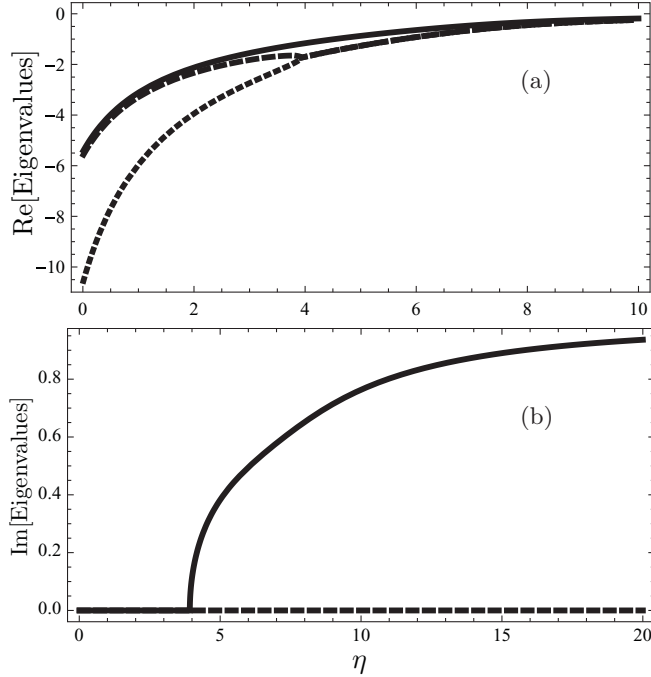


FIG. 7. The magnitude of the real (a) and imaginary (b) components of the eigenvalues of the system (50) linearized about its steady state, as a function of η . In (b), the solid and dashed curves represent the magnitude of the two unique imaginary components. The remaining parameters are $\Lambda = 10$, $S = 1$, $\delta_m = 1$, and $Mn = 1$.

depends on the other physical parameters in addition to the excess area Δ . Finally, note that this linear stability analysis yields results consistent with the numerical solution of the system as presented in Figs. 5 and 6.

VI. CONCLUSIONS

In this study we considered the effects of a steady uniform electric field on the dynamics of a vesicle in a simple shear flow. We have developed a model which accounts for the fluidity and incompressibility of the interface in addition to bending resistance. The interface is treated as a capacitor and thus the boundary conditions at the membrane have intrinsic time dependence. In the limit of a nearly spherical vesicle and weak electric field, we derived a system of coupled nonlinear ordinary differential equations with time-dependent coefficients which describe the evolution of the vesicle shape.

The solution of the evolution equations shows that in the absence of an applied shear flow, the vesicle either remains a prolate ellipsoid at all times, or temporarily enters an oblate state before becoming prolate. The oblate-prolate transition is related to the charging of the membrane capacitor. Initially the vesicle interior participates in the conduction process because of the displacement current through the membrane. Vesicle deformation is determined by the polarization, which depends on the ratio of conductivities between the inner and outer fluids. If the inner fluid is less conducting than the exterior solution, the induced dipole is directed oppositely to the applied field and the resulting deformation is oblate. Once the capacitor is

fully charged, the electric field is expelled from the interior and the vesicle deforms as an ideally polarizable particle into a prolate ellipsoid.

In the absence of electric field, at low viscosity ratios, the torque of the applied shear flow is transmitted via the TT membrane into circulation of the interior fluid and the vesicle assumes a stationary TT state. However, at high interior fluid viscosity the fluid flows less readily. When the viscosity ratio becomes sufficiently large, the stress exerted by the flow is no longer sufficient to drive the TT motion while preserving area incompressibility, the membrane becomes solidlike and the vesicle tumbles. The electric field exerts additional stress on the membrane which aids TT.

Our theoretical results are consistent with available experimental data [19], albeit some of the theoretical predictions such as the oblate-prolate transition in absence of applied flow and the suppressed tumbling under shear when an electric field is present remain to be experimentally tested. Another interesting problem is the effect of thermal fluctuations on the morphological transitions.

ACKNOWLEDGMENTS

J.T.S. and M.J.M. acknowledge financial support by NSF RTG Grant No. DMS-0636574 and NSF Grant No. DMS-0616468. P.M.V. acknowledges partial financial support by NSF Grant No. CBET-0846247.

APPENDIX A: FORCING TERM FROM THE ELECTRIC FIELD IN THE SHAPE EVOLUTION EQUATION

For an electric field in the z direction,

$$C_{20}^{\text{el}} = \frac{4\sqrt{5\pi}}{5(32 + 23\eta)} \Xi(t), \quad (\text{A1})$$

and for an electric field in the y direction,

$$C_{20}^{\text{el}} = \sqrt{\frac{2}{3}} C_{2\pm 2}^{\text{el}} = -\frac{2\sqrt{5\pi}}{5(32 + 23\eta)} \Xi(t), \quad (\text{A2})$$

where

$$\Xi(t) = -4SP_{\text{in}}^2 + (-2 + P_{\text{ex}})^2 = \frac{1}{(\Lambda + 2)^2} [(\Lambda \bar{V}(t) - 3(\Lambda + 1))^2 - 4S(3 - 2\bar{V}(t))^2]. \quad (\text{A3})$$

The amplitude of the transmembrane potential $\bar{V}(t)$ is given by Eq. (30).

APPENDIX B: FURTHER RESULTS FOR VESICLE DYNAMICS IN ELECTRIC FIELDS

Expressions for the constants B_k in $J(t)$ are

$$\begin{aligned} B_1 &= 9\sqrt{5\pi}/[5(32 + 23\eta)(2 + \Lambda)^2], \\ B_2 &= -16S + \Lambda(8 + 5\Lambda), \quad B_3 = 2(2 + \Lambda)^2, \\ B_4 &= 16S - \Lambda^2, \quad B_5 = 4\Lambda(2 + \Lambda). \end{aligned} \quad (\text{B1})$$

The stationary solution shown in (44) (which defines a prolate vesicle) was obtained at by examining long-time behavior of (42). It can also be derived by assuming that

the time-dependent forcing from the electric field, $C_{20}^{\text{el}}(t)$ has reached its steady state, which makes Eqs. (41) autonomous. Introducing the constant quantity, $C_{20}^{\text{el}\infty} = C_{20}^{\text{el}}(t = \infty)$, setting the left-hand side of (41) to zero, and solving for f_{20} yields (44). However, a second stationary solution also exists,

$$f_{20}^{\text{min}} = -\sqrt{\frac{\Delta}{2}}. \quad (\text{B2})$$

This solution corresponds to an oblate spheroid. Linearizing the system (41) about the prolate solution (44) and performing a stability analysis reveals real, negative eigenvalues $\omega_1 = -C_{20}^{\text{el}\infty}\sqrt{\Delta/2}$ and $\omega_2 = 2\omega_1$. This indicates that the prolate state is characterized by a stable node at long times. On the other hand, if the evolution equations (41) were linearized about the oblate state (B2), the eigenvalues are positive, which shows that at long times, the oblate state is an unstable solution.

Lastly, if one were to freeze time in $C_{20}^{\text{el}}(t)$ at $t = 0$, and not the long-time state, the signs on the eigenvalues switch depending on the value of Λ . In particular, if $\Lambda < 1$ and $C_{20}^{\text{el}}(0)$ is negative, the equilibrium solution (B2) is stable, and hence initially an attractor. On the other hand, if $\Lambda > 1$ and $C_{20}^{\text{el}}(0)$ is positive, then (44) is the attractor. These predictions are consistent with the dynamics shown in Fig. 4.

APPENDIX C: ELECTRIC FIELD ALONG THE VORTICITY DIRECTION

Orientation of the electric field along other coordinate axes results in similar time-dependent dynamics of the shape modes seen in Fig. 6, i.e., the vesicle undergoes a damped tumbling motion. We should note that when the electric field is directed along the z coordinate axis ($\alpha = 0$, $\beta = 1$) [see (26)], the system reduces to a more compact form. Steady states can be analytically obtained from (50) by solving

$$0 = -\Delta f_{22}'' + 2f_{22}'(2C_{22}^{\text{shear}} f_{22}'' - C_{20}^{\text{el}} f_{20}), \quad (\text{C1})$$

$$0 = \Delta(f_{22}' + C_{22}^{\text{shear}}) + 2f_{22}''(2C_{22}^{\text{shear}} f_{22}'' - C_{20}^{\text{el}} f_{20}), \quad (\text{C2})$$

$$0 = 4C_{22}^{\text{shear}} f_{20} f_{22}'' + C_{20}^{\text{el}}(\Delta - 2f_{20}^2), \quad (\text{C3})$$

for f_{22}' , f_{22}'' , and f_{20} . Note that one must also assume the time-dependent coefficients have reached their steady state. A fourth order polynomial for f_{20} is found,

$$2f_{20}^4 + [2(C_{20}^{\text{el}})^2 + 4C_{22}^{\text{shear}} - \Delta]f_{20}^2 - \Delta(C_{20}^{\text{el}})^2 = 0. \quad (\text{C4})$$

The four steady states of f_{20} are

$$f_{20} = \pm \frac{1}{2}[-2(C_{20}^{\text{el}})^2 - \gamma - \zeta]^{1/2} \quad (\text{C5})$$

and

$$f_{20} = \pm \frac{1}{2}[-2(C_{20}^{\text{el}})^2 + \gamma + \zeta]^{1/2}, \quad (\text{C6})$$

where $\gamma = 4(C_{22}^{\text{shear}})^2 - \Delta$, and

$$\zeta = [8\Delta(C_{20}^{\text{el}})^2 + (2(C_{20}^{\text{el}})^2 + \gamma)^2]^{1/2}. \quad (\text{C7})$$

The two solutions given by (C5) are imaginary for physical values of the parameters, and therefore are not valid. The two solutions given by (C6) are real, and therefore valid solutions of the system. We linearize the evolution Equation (50) about the solutions given by (C6), and with the corresponding f_{22}' and f_{22}'' [found from (C9) and (C8), respectively]. The eigenvalues in this system are complex with either a positive or negative real part, depending on the sign taken for f_{20} from (C6); adopting the positive sign for f_{20} yields a stable system.

From (C1), the steady state of f_{22}'' is found to be

$$f_{22}'' = \frac{C_{20}^{\text{el}}(2f_{20}^2 - \Delta)}{4C_{22}^{\text{shear}} f_{20}}. \quad (\text{C8})$$

Additionally, using (C2), the expression for f_{22}' can be found,

$$f_{22}' = \frac{\Delta f_{22}''}{2C_{20}^{\text{el}} f_{20} - 4C_{22}^{\text{shear}} f_{22}''}. \quad (\text{C9})$$

Inserting (C8) into (C9) and using (C3) yields (C4).

APPENDIX D: SPHERICAL HARMONICS

The normalized scalar spherical harmonics are defined as

$$Y_{jn}(\theta, \phi) = \left[\frac{2j+1}{4\pi} \frac{(j-n)!}{(j+n)!} \right]^{\frac{1}{2}} (-1)^n P_j^n(\cos \theta) e^{in\phi}, \quad (\text{D1})$$

where $P_j^n(\cos \theta)$ are the associated Legendre polynomials. For example,

$$Y_{10} = \sqrt{\frac{3}{4\pi}} \cos \theta. \quad (\text{D2})$$

The vector spherical harmonics relevant to our study are defined as [57]

$$\begin{aligned} \mathbf{y}_{jn0} &= [j(j+1)]^{-1/2} r \nabla_{\Omega} Y_{jn}, \\ \mathbf{y}_{jn1} &= -i\hat{\mathbf{r}} \times \mathbf{y}_{jn0}, \quad \mathbf{y}_{jn2} = \hat{\mathbf{r}} Y_{jn}. \end{aligned} \quad (\text{D3})$$

For example

$$\mathbf{y}_{200} = -\sqrt{\frac{15}{32\pi}} \sin(2\theta) \mathbf{e}_{\theta}, \quad \mathbf{y}_{202} = \frac{1}{8} \sqrt{\frac{5}{\pi}} [1 + 3 \cos(2\theta)] \hat{\mathbf{r}}, \quad (\text{D4})$$

$$\mathbf{y}_{222} + \mathbf{y}_{2-22} = \sqrt{\frac{15}{8\pi}} (\cos 2\phi \sin^2 \theta) \hat{\mathbf{r}}, \quad (\text{D5})$$

$$\mathbf{y}_{220} + \mathbf{y}_{2-20} = \sqrt{\frac{5}{4\pi}} \left[\frac{1}{2} (\cos 2\phi \sin 2\theta) \mathbf{e}_{\theta} - (\sin 2\phi \sin \theta) \mathbf{e}_{\phi} \right]. \quad (\text{D6})$$

Calculations of the electric tractions involve recoupling of products of vector and scalar spherical harmonics. A detailed presentation of general recoupling formulas is beyond the scope of this paper and can be found in Ref. [58]. Here we

list the formulas needed to complete the calculation in this work:

$$Y_{1\pm 1}Y_{1\pm 1} = \sqrt{\frac{3}{10\pi}}Y_{2\pm 2}, \quad (D7a)$$

$$Y_{1-1}Y_{11} = -\frac{1}{2\sqrt{\pi}}Y_{00} + \frac{1}{2\sqrt{5\pi}}Y_{20}.$$

$$\sqrt{2}Y_{1\pm 1}\mathbf{y}_{1\pm 10} = \frac{1}{2\sqrt{10\pi}}\mathbf{y}_{2\pm 2}, \quad (D7b)$$

$$\sqrt{2}Y_{1\pm 1}\mathbf{y}_{1\mp 10} = \mp \frac{1}{2}\sqrt{\frac{3}{2\pi}}\mathbf{y}_{101} + \frac{1}{4}\sqrt{\frac{3}{5\pi}}\mathbf{y}_{200}.$$

$$2\mathbf{y}_{1\pm 10} \cdot \mathbf{y}_{1\pm 10} = -\sqrt{\frac{3}{10\pi}}Y_{2\pm 2}, \quad (D7c)$$

$$2\mathbf{y}_{1-10} \cdot \mathbf{y}_{110} = -\frac{1}{\sqrt{\pi}}Y_{00} + \frac{1}{\sqrt{5\pi}}Y_{20}.$$

APPENDIX E: VESICLE DEFORMATION IN EXTERNAL FIELD: SOLUTION

Here we outline the solution for the velocity field resulting from electric tractions in the case of a sphere placed in an uniform electric field. More details can be found in Refs. [26–28,40,59]. The formalism was originally developed to study droplets in flow [58,60,61].

Velocity fields are described using basis sets of fundamental solutions of the Stokes equations appropriate for spherical geometry [62], \mathbf{u}_{jm}^{\pm} , defined in Appendix F:

$$\mathbf{v}^{\text{ex}}(\mathbf{r}) = \sum_{jm} c_{jm} \mathbf{u}_{jm}^{-}(\mathbf{r}), \quad \mathbf{v}^{\text{in}}(\mathbf{r}) = \sum_{jm} c_{jm} \mathbf{u}_{jm}^{+}(\mathbf{r}). \quad (E1)$$

$$\sum_{jm} \equiv \sum_{j=2}^{\infty} \sum_{m=-j}^j \sum_{q=0}^2, \quad (E2)$$

$$\Sigma(\theta, \phi, t) = \Sigma_h + \sum_{j \geq 2} \sum_{m=-j}^j \Sigma_{jm}(t) Y_{jm}, \quad (E3)$$

where Σ_h is the isotropic part of the tension used to enforce a global constraint on the area. The local area conservation implies that the velocity field at the interface is solenoidal [40],

$$\nabla_s \cdot \mathbf{v} = 0. \quad (E4)$$

Therefore the amplitudes of the velocity field (E1) are related:

$$c_{jm0} = \frac{2}{\sqrt{j(j+1)}} c_{jm2}. \quad (E5)$$

The component of velocity that is normal to the interface, c_{jm2} , is determined using the stress balance, which in terms of spherical harmonics reads

$$\delta_{j2} \delta_{m0} \tau_{jm}^{\text{el}} + \tau_{jm}^{\text{hd,ex}} - \eta \tau_{jm}^{\text{hd,in}} = \text{Ca}^{-1} \tau_{jm}^{\text{m}}. \quad (E6)$$

Tangential stresses correspond to the $q = 0$ component, and the normal stresses to $q = 2$. δ_{ij} is the Kronecker delta function. The hydrodynamic tractions are given by (F6)–(F9). The electrical tractions are given by (see Sec. III C)

$$\tau^{\text{el}} = 8\sqrt{\frac{\pi}{5}} P^{\text{el}} \mathbf{y}_{202}(\theta, \phi) - 2\sqrt{\frac{2\pi}{15}} \tau_s^{\text{el}} \mathbf{y}_{200}(\theta, \phi). \quad (E7)$$

The membrane tractions are [26,40]

$$\tau_{jm}^{\text{m}} = \tau_{jm}^{\kappa} + \tau_{jm}^{\Sigma}. \quad (E8)$$

The bending contribution to the membrane traction is

$$\tau_{jm}^{\kappa} = j(j+1)(j-1)(j+2)f_{jm}, \quad \tau_{jm0}^{\kappa} = 0, \quad (E9)$$

the stresses due to membrane tension are

$$\tau_{jm}^{\Sigma} = 2\Sigma_{jm} + \Sigma_h(j-1)(j+2)f_{jm}, \quad (E10)$$

$$\tau_{jm0}^{\Sigma} = -\sqrt{j(j+1)}\Sigma_{jm}.$$

The nonuniform part of the membrane tension, Σ_{jm} , is determined from the tangential component of the stress balance (E6), $q = 0$,

$$\Sigma_{jm} = \text{Ca} \left[\frac{\tau_{jm0}^{\text{el}}}{\sqrt{j(j+1)}} + c_{jm2} \frac{2+j+(j-1)\eta}{j(j+1)} \right]. \quad (E11)$$

It is then substituted into the normal component of the stress balance (E6), $q = 2$, to obtain the normal velocity c_{jm2} ,

$$c_{jm2} = C_{jm} + \text{Ca}^{-1}(\Gamma_1 + \Sigma_h \Gamma_2) f_{jm}, \quad (E12)$$

where

$$C_{jm} = -\frac{\sqrt{j(j+1)}}{d(\eta, j)} [2\tau_{jm0}^{\text{el}} + \sqrt{j(j+1)}\tau_{jm2}^{\text{el}}], \quad (E13)$$

$$\Gamma_1 = -(j+2)(j-1)[j(j+1)]^2 d(\eta, j)^{-1}, \quad (E14)$$

$$\Gamma_2 = -(j+2)(j-1)j(j+1) d(\eta, j)^{-1}, \quad (E15)$$

and

$$d(\eta, j) = (4 + 3j^2 + 2j^3) + (-5 + 3j^2 + 2j^3)\eta. \quad (E16)$$

Finally, the motion of the interface is determined from the kinematic condition (12),

$$\frac{\partial f_{jm}}{\partial t} = c_{jm2} + \frac{im}{2} f_{jm} \quad \text{at } r = 1. \quad (E17)$$

Substituting c_{jm2} in (E17) yields the evolution equation for the shape parameters (38),

$$\Sigma_h = -\frac{\sum_{jm} a(j)[C_{jm} f_{jm}^* + \text{Ca}^{-1} \Gamma_1 f_{jm} f_{jm}^*]}{\text{Ca}^{-1} \sum_{jm} a(j) \Gamma_2 f_{jm} f_{jm}^*}, \quad (E18)$$

where

$$a(j) = \frac{1}{2}(j+2)(j-1). \quad (E19)$$

The normal velocity (E12) and the shape evolution (E17) include the yet unknown isotropic membrane tension. It is expressed in terms of the shape modes and other known parameters in the problem using the area constraint [26].

The complicated dependence of the tension on the shape modes makes the shape evolution equations nonlinear.

In order to clarify the physical significance of the isotropic tension, let us consider the particular case when only the ellipsoidal deformation modes, $j = 2$, are present. (E18) simplifies to

$$\Sigma_h(t) = -6 + \text{Ca} \frac{32 + 23\eta}{12} [C_{20} f_{20}(t) + C_{22} f_{2-2}(t) + C_{2-2} f_{22}(t)], \quad (E20)$$

where we have emphasized that the time-dependent shape modes give rise to time-dependent membrane tension. We see that the tension varies with deformation.

In absence of applied shear, and electric field along the z axis, once all excess area is transferred to the f_{20} mode, the tension increases with the field strength Ca as

$$\Sigma_h \approx Ca C_{20} \frac{(32 + 23\eta)\sqrt{2}}{12} \Delta^{-1/2} \quad (\text{E21})$$

APPENDIX F: FUNDAMENTAL SET OF VELOCITY FIELDS

Following the definitions given in Blawdziewicz *et al.* [57], we list the expressions for the functions $\mathbf{u}_{jm}^\pm(r, \theta, \varphi)$. The velocity field outside the vesicle is described by

$$\begin{aligned} \mathbf{u}_{jm0}^- &= \frac{1}{2} r^{-j} (2 - j + j r^{-2}) \mathbf{y}_{jm0} \\ &+ \frac{1}{2} r^{-j} [j(j+1)]^{1/2} (1 - r^{-2}) \mathbf{y}_{jm2}, \end{aligned} \quad (\text{F1})$$

$$\begin{aligned} \mathbf{u}_{jm2}^- &= \frac{1}{2} r^{-j} (2 - j) \left(\frac{j}{1+j} \right)^{1/2} (1 - r^{-2}) \mathbf{y}_{jm0} \\ &+ \frac{1}{2} r^{-j} (j + (2 - j)r^{-2}) \mathbf{y}_{jm2}. \end{aligned} \quad (\text{F2})$$

The velocity field inside the vesicle is described by

$$\begin{aligned} \mathbf{u}_{jm0}^+ &= \frac{1}{2} r^{j-1} (-(j+1) + (j+3)r^2) \mathbf{y}_{jm0} \\ &- \frac{1}{2} r^{j-1} [j(j+1)]^{1/2} (1 - r^2) \mathbf{y}_{jm2}, \end{aligned} \quad (\text{F3})$$

$$\begin{aligned} \mathbf{u}_{jm2}^+ &= \frac{1}{2} r^{j-1} (3 + j) \left(\frac{j+1}{j} \right)^{1/2} (1 - r^2) \mathbf{y}_{jm0} \\ &+ \frac{1}{2} r^{j-1} (j + 3 - (j+1)r^2) \mathbf{y}_{jm2}. \end{aligned} \quad (\text{F4})$$

On a sphere $r = 1$ these velocity fields reduce to the vector spherical harmonics defined by (D3),

$$\mathbf{u}_{jm}^\pm = \mathbf{y}_{jm}. \quad (\text{F5})$$

Hence, \mathbf{u}_{jm0}^\pm is tangential, and \mathbf{u}_{jm2}^\pm is normal to a sphere. In addition, \mathbf{u}_{jm0}^\pm defines an irrotational velocity field.

The hydrodynamic tractions associated with the velocity fields (E1) are [26]

$$\tau_{jm0}^{\text{hd, in}} = (2j+1)c_{jm0} - 3 \left(\frac{j+1}{j} \right)^{1/2} c_{jm2}, \quad (\text{F6})$$

$$\tau_{jm0}^{\text{hd, ex}} = -(2j+1)c_{jm0} + 3 \left(\frac{j}{j+1} \right)^{1/2} c_{jm2}, \quad (\text{F7})$$

$$\tau_{jm2}^{\text{hd, ex}} = 3 \left(\frac{j}{j+1} \right)^{1/2} c_{jm0} - \frac{4+3j+2j^2}{j+1} c_{jm2}, \quad (\text{F8})$$

$$\tau_{jm2}^{\text{hd, in}} = -3 \left(\frac{j+1}{j} \right)^{1/2} c_{jm0} + \frac{3+j+2j^2}{j} c_{jm2}. \quad (\text{F9})$$

-
- [1] B. Alberts, A. Johnson, J. Lewis, M. Raff, K. Roberts, and P. Walter, *Molecular Biology of the Cell*, 4th ed. (Garland, New York, 2002).
- [2] P. Walde, *Bioessays* **32**, 296 (2010).
- [3] R. Dimova, S. Aranda, N. Bezlyepkina, V. Nikolov, K. A. Riske, and R. Lipowsky, *J. Phys. Condens. Matter* **18**, S1151 (2006).
- [4] M. Abkarian and A. Viallat, *Soft Matter* **4**, 653 (2008).
- [5] P. M. Vlahovska, T. Podgorski, and M. Misbah, *C. R. Phys.* **10**, 775 (2009).
- [6] R. Dimova, N. Bezlyepkina, M. D. Jord, R. L. Knorr, K. A. Riske, M. Staykova, P. M. Vlahovska, T. Yamamoto, P. Yang, and R. Lipowsky, *Soft Matter* **5**, 3201 (2009).
- [7] P. M. Vlahovska, in *Advances in Planar Lipid Bilayers and Liposomes*, edited by Iglic and Tien, vol. 12 (Elsevier, Amsterdam, 2010), pp. 101–146.
- [8] M. Karlsson, M. Davidson, R. Karlsson, A. Karlsson, J. Bergenholtz, Z. Konkoli, A. Jesorka, T. Lobovkina, J. Hurtig, M. Voinova, and O. Orwar, *Ann. Rev. Phys. Chem.* **55**, 613 (2004).
- [9] V. Kantsler and V. Steinberg, *Phys. Rev. Lett.* **95**, 258101 (2005).
- [10] V. Kantsler and V. Steinberg, *Phys. Rev. Lett.* **96**, 036001 (2006).
- [11] M.-A. Mader, V. Vitkova, M. Abkarian, A. Viallat, and T. Podgorski, *Eur. Phys. J. E* **19**, 389 (2006).
- [12] J. Deschamps, V. Kantsler, and V. Steinberg, *Phys. Rev. Lett.* **102**, 118105 (2009).
- [13] J. Deschamps, V. Kantsler, E. Segre, and V. Steinberg, *Proc. Natl. Acad. Sci. USA* **106**, 11444 (2009).
- [14] M. Kummrow and W. Helfrich, *Phys. Rev. A* **44**, 8356 (1991).
- [15] M. D. Mitov, P. Meleard, M. Winterhalter, M. I. Angelova, and P. Bothorel, *Phys. Rev. E* **48**, 628 (1993).
- [16] K. A. Riske and R. Dimova, *Biophys. J.* **88**, 1143 (2005).
- [17] S. Aranda, K. A. Riske, R. Lipowsky, and R. Dimova, *Biophys. J.* **95**, L19 (2008).
- [18] K. Antonova, V. Vitkova, and M. D. Mitov, *Europhys. Lett.* **89**, 38004 (2010).
- [19] K. A. Riske and R. Dimova, *Biophys. J.* **91**, 1778 (2006).
- [20] R. S. Allan and S. G. Mason, *Proc. R. Soc. London, Ser. A* **267**, 45 (1962).
- [21] J. W. Ha and S. M. Yang, *Phys. Fluids* **12**, 1671 (2000).
- [22] S. Mahlmann and D. T. Papageorgiou, *J. Fluid Mech.* **626**, 367 (2009).
- [23] P. M. Vlahovska, *J. Fluid Mech.* **670**, 481 (2011).
- [24] P. M. Vlahovska, R. S. Gracia, S. Aranda-Espinoza, and R. Dimova, *Biophys. J.* **96**, 4789 (2009).
- [25] C. Misbah, *Phys. Rev. Lett.* **96**, 028104 (2006).
- [26] P. M. Vlahovska and R. S. Gracia, *Phys. Rev. E* **75**, 016313 (2007).
- [27] V. V. Lebedev, K. S. Turitsyn, and S. S. Vergeles, *New J. Phys.* **10**, 043044 (2008).
- [28] J. Schwalbe, P. M. Vlahovska, and M. Miksis, *J. Fluid Mech.* **647**, 403 (2010).
- [29] M. A. Lomholt and L. Miao, *J. Phys. A* **39**, 10323 (2006).
- [30] W. Helfrich, *Z. Naturforsch. C* **28**, 693 (1973).
- [31] P. B. Canham, *J. Theor. Biol.* **26**, 61 (1970).

- [32] U. Seifert, *Adv. Phys.* **46**, 13 (1997).
- [33] J. R. Melcher and G. I. Taylor, *Annu. Rev. Fluid Mech.* **1**, 111 (1969).
- [34] D. A. Saville, *Annu. Rev. Fluid Mech.* **29**, 27 (1997).
- [35] T. B. Jones, *Electromechanics of Particles* (Cambridge University Press, New York, 1995).
- [36] G. I. Taylor, *Proc. R. Soc. London, Ser. A* **291**, 159 (1966).
- [37] C. Grosse and H. P. Schwan, *Biophys. J.* **63**, 1632 (1992).
- [38] H. P. Schwan, in *Electroporation and Electrofusion in Cell Biology*, edited by E. Neumann, A. E. Sowers, and C. A. Jordan (Plenum, New York, 1989), pp. 3–21.
- [39] K. Kinoshita Jr., I. Ashikawa, N. Saita, H. Yoshimura, H. Itoh, K. Nagayama, and A. Ikegami, *Biophys. J.* **53**, 1015 (1988).
- [40] U. Seifert, *Eur. Phys. J. B* **8**, 405 (1999).
- [41] R. Dimova, K. A. Riske, S. Aranda, N. Bezlyepkina, R. L. Knorr, and R. Lipowsky, *Soft matter* **3**, 817 (2007).
- [42] T. Portet, F. C. I. Febrer, J. M. Escoffre, C. Favard, M. P. Rols, and D. S. Dean, *Biophys. J.* **96**, 4109 (2009).
- [43] K. A. Riske, R. L. Knorr, and R. Dimova, *Soft Matter* **5**, 1983 (2009).
- [44] R. S. Gracia, N. Bezlyepkina, R. L. Knorr, R. L. Lipowsky, and R. Dimova, *Soft Matter* **6**, 1472 (2010).
- [45] T. Portet and R. Dimova, *Biophys. J.* **99**, 3264 (2010).
- [46] R. L. Knorr, M. Staykova, R. S. Gracia, and R. Dimova, *Soft Matter* **6**, 1990 (2010).
- [47] D. Needham and R. M. Hochmuth, *Biophys. J.* **55**, 1001 (1989).
- [48] V. Kantsler, E. Segre, and V. Steinberg, *Europhys. Lett.* **82**, 58005 (2008).
- [49] V. Vitkova, M. Mader, B. Polack, C. Misbah, and T. Podgorski, *Biophys. J.* **95**, L33 (2008).
- [50] G. Couplier, B. Kaoui, T. Podgorski, and C. Misbah, *Phys. Fluids* **20**, 111702 (2008).
- [51] N. Callens, C. Minetti, G. Couplier, M.-A. Mader, F. Dubois, C. Misbah, and T. Podgorski, *Europhys. Lett.* **83**, 24002 (2008).
- [52] W. Krassowska and P. D. Filev, *Biophys. J.* **92**, 404 (2007).
- [53] J. Schwalbe, Ph.D. thesis, Northwestern University, 2010.
- [54] T. Yamamoto, S. Aranda-Espinoza, R. Dimova, and R. Lipowsky, *Langmuir* **26**, 12390 (2010).
- [55] P. Peterlin, *J. Biol. Phys.* **36**, 339 (2010).
- [56] S. R. Keller and R. Skalak, *J. Fluid Mech.* **120**, 27 (1982).
- [57] J. Bławdziewicz, P. Vlahovska, and M. Loewenberg *Physica A* **276**, 50 (2000).
- [58] P. Vlahovska, J. Bławdziewicz, and M. Loewenberg *Phys. Fluids* **17**, 103103 (2005).
- [59] G. Danker, T. Biben, T. Podgorski, C. Verdier, and C. Misbah, *Phys. Rev. E* **76**, 041905 (2007).
- [60] P. M. Vlahovska, Ph.D. thesis, Yale University, 2003 (PDF file available by email: [petia@aya.yale.edu]).
- [61] P. Vlahovska, J. Bławdziewicz, and M. Loewenberg, *J. Fluid Mech.* **624**, 293 (2009).
- [62] B. Cichocki, B. U. Felderhof, and R. Schmitz, *PhysicoChem. Hyd.* **10**, 383 (1988).